

Density functional calculation of the heats of formation of rare-earth orthophosphates

James R. Rustad, Sullivan Park Research Center. Corning, Inc., Corning, NY 14831

Abstract

Electronic structure calculations are carried out to estimate the heats of formation of rare-earth orthophosphates from their oxides. The calculated heats of formation are systematically about 40 kJ/mol less exothermic than the measured values. Based on estimated corrections for zero-point energies and $H(298.15)-H(0)$, the discrepancy is almost entirely electronic in origin. The decreasingly exothermic $\Delta H_{\text{ox}}^{\text{f}}$ with decreasing ionic radius (i.e. LaPO_4 more exothermic than ScPO_4) results from the higher charge localization on the oxide anion (O^{2-}) relative to the phosphate anion (PO_4^{3-}). The lattice energy, of course, becomes more negative with decreasing ionic radius for both oxide and phosphate phases, but does so more rapidly for the oxide, making the reaction less exothermic as ionic radius becomes smaller. This effect should carry over to $\Delta H_{\text{ox}}^{\text{f}}$ other oxyacids, such as silicates and sulfates.

Introduction

The rare-earth (RE) phosphates are versatile refractory materials with a wide range of geological and technological applications (Ushakov et al., 2002). This paper reports the results of a series of density-functional electronic structure calculations of the thermodynamic properties of rare-earth phosphates. The purpose of the paper is to determine how well the calculated heats of formation from the oxides match measured values, and to compare the potential sources of error coming from lattice thermal contributions to the enthalpy, zero-point energies, and electronic energies.

This information is important for several reasons. First, it is only through studies of a systematic series of minerals that better density functionals for thermal properties can be developed. Studies focused only on individual phases cannot uncover systematic trends that are essential for making these improvements. Second, studies of interfacial properties of these minerals, in contact with both aqueous and silicate solvents, will require construction of potential functions (Pedone et al., 2006). While it is common to

use structural and elastic properties to construct these potential functions, energetics of reactions such as heats of formation from the oxides $\Delta H_{\text{ox}}^{\text{f}}$ (298.15K), (e.g. $\frac{1}{2}\text{Ln}_2\text{O}_3 + \frac{1}{2}\text{P}_2\text{O}_5 = \text{LnPO}_4$) are often not considered, mainly because the reported $\Delta H_{\text{ox}}^{\text{f}}$ will contain zero-point and enthalpic temperature corrections which cannot be made until vibrational analysis is carried out. Tables of electronic heats of formation at zero temperature, if available (and accurate, of course) would aid in the construction of transferable potential functions, which may eventually be capable of predicting thermodynamic properties of complex mixtures, such as glasses and melts. While interfacial phenomena in mineral-aqueous systems are well explored using simulation techniques, little work has been done on simulation of melt-crystal interfaces (Gurmani et al., 2010). Molecular processes at magma-mineral interfaces will require correct thermodynamics for reactions such as $2\text{LaPO}_4 = \text{La}_2\text{O}_3(\text{s}) + \text{P}_2\text{O}_5(\text{melt})$. While obtaining the free energy of dissolution of P_2O_5 in a silicate melt will be out of reach of first-principles simulations methods for some time, it may be possible to obtain correct trends with parameterized potential functions, if they have been developed with attention paid to obtaining correct energetics. It is hoped that input on formation energies from first-principles methods will facilitate these efforts.

Methods

Electronic structure calculations are carried out with density functional theory (DFT) using the Projector Augmented Wave (PAW) method (Blochl, 1994) implemented in VASP 4.6.11 (Kresse and Furthmuller, 1996; Kresse and Hafner, 1993), with PAW pseudopotentials (Kresse and Joubert, 1999) constructed for the PBE exchange correlation functional (Perdew et al., 1996). The calculations on the lanthanide elements use the Ln_3 trivalent lanthanide pseudopotentials. These provide an implicit treatment of the *f* electron shell across the series of rare earth elements. Calculations for yttrium and scandium use the Y_sv and Sc_sv pseudopotentials. LuPO_4 failed to achieve SCF convergence, so this was eliminated from the study, along with Eu, Pm, and Yb. DFT+U calculations are carried for Ce_2O_3 and CePO_4 using the standard Ce PBE pseudopotential and a U value of 3 eV, which was found to be an optimal value both for Ce_2O_3 (Fabris et al., 2005; Loschen et al, 2007) and CePO_4 (Adelstein et al., 2011). The DFT+U calculations use the method of Dudarev et al (1998).

The cutoff energy was set to 500 eV for all systems. A gamma-centered reciprocal space grid was used for each system. The following k-point grid sizes were used: For the C-oxide, monazite, and xenotime structures, 7 x 7 x 7; for the A-oxide structures, 15x15x15; for *h*-P₄O₁₀ and *o'*-P₂O₅, 7x7x7. Structure optimizations were done with both volume and lattice vectors varying simultaneously. Final structures were run with no optimization to ensure that the absolute value of the pressure was below 0.1 GPa. Final configurations outside this range were optimized again until the pressure criterion was satisfied.

Results and Discussion

Structure and Energetics of RE₂O₃ Oxides

Tables 1, 2, and 3 give the optimized structural parameters and molar volume for some RE₂O₃ oxides, along with values obtained from x-ray measurements (Koehler and Wollan, 1953; Fert, 1962; Hase, 1963; Knop and Hartley, 1963; Boulesteix et al. 1971; Bourcherle et al., 1975; Saiki et al., 1985; Schiller, 1985; Bartos et al., 1993 Greis, 1994 ; Baldinozzi et al., 1998; Kuemmerle and Heger, 1999; Zhang et al., 2008). The large rare-earth oxides La₂O₃, Ce₂O₃, Nd₂O₃, and Pr₂O₃ are known to be most stable in the hexagonal A-type structure. Previous work (Wu et al. 2007) compared the electronic energies of a series of rare-earth oxides in the A and monoclinic B-type structure using the same method used here (PAW-PBE), but did not report results for the cubic C-type structure. An earlier PAW-GGA study (Hirosaki et al., 2003) gave structures but not energies for the C-type oxides. Table 4 gives the calculated energies for the suite of RE oxide compounds in the C-type structure as well as the A-type structure for La, Ce, Nd, and Pr, and the B-type structure for Sm and Gd. The results are very close to those previously calculated. The results show that PAW-PBE predicts (incorrectly) that La, Ce, Nd, Pr, and Sm are most stable in the C-type structure. This was already noted for Ce₂O₃ (Da Silva, 2007). As shown in Tables 1-3, calculated molar volumes are generally 2-3 percent greater than measured values, except for A-Ce₂O₃, which is 4.8 percent above the measured value. The PAW PBE+U calculations give improved calculations of the volume and lattice parameters for the A- and C-Ce₂O₃ phases. They are also reported to

stabilize A-type Ce_2O_3 over C-type Ce_2O_3 (Da Silva, 2007) (DFT+U calculations were not done on C- Ce_2O_3 here).

Structures and Energetics of REPO₄ Phosphates

Tables 5 (xenotime) and 6 (monazite) give the optimized structural parameters and calculated energies per formula unit for the RE orthophosphates. Comparisons are made with the x-ray measurements (Ni et al., 1995; Milligan et al., 1982). The data overestimate volumes by close to 2% for the monazite-type REPO₄, and 2-3% for the xenotime REPO₄, except for CePO₄(m) which is overestimated by 4.6% with PBE and Ce_3 pseudopotential. The structure is improved slightly in the PBE+U treatment. In other respects, the structural calculations are unremarkable and in line with those of the oxides.

Calculated electronic energies for the REPO₄ are given in Table 7. La, Ce, Pr, and Nd are all most stable in the monazite structure, in agreement with observations (although actual measured values for ΔG of the monazite-xenotime polymorphs are not available for any of the REPO₄). For NdPO₄, the monazite and xenotime structures are nearly isoenergetic. For Tb-Tm, as well as Sc and Y, the xenotime structure is most stable, also in line with observations. SmPO₄ and GdPO₄ are also calculated to be more stable in the xenotime structure. The PBE+U calculations on CePO₄ give a low-energy antiferromagnetic structure almost isoenergetic with the ferromagnetic solution. The PBE+U treatment increases the stabilization of FM-CePO₄(m) relative to FM-CePO₄(x) by about 20 kJ/mol.

Structures and Energetics of P₂O₅

For calculation of the electronic energies of formation from the oxides, the total energy of P₂O₅ is needed. In the study of Ushakov et al. (2002), the P₂O₅ phase was the hexagonal *h*-P₂O₅. This is a molecular solid having discrete adamantane-like P₄O₁₀ molecules held together by van der Waals interactions which are not accounted for in the DFT. The omission of this contribution to the cohesive energy of P₂O₅ will produce a systematic error in the calculations, with the calculated $\Delta E_{\text{e ox}}^{\text{f}}$ being consistently too

negative. It is known that the *h*-P₂O₅ phase is metastable with respect to a polymeric (i.e. non-molecular) orthorhombic *o'*-P₂O₅ compound (Greenwood and Earnshaw, 1985) in which molecular Van der Waals forces presumably play no role. As an upper bound to the required correction, it could be assumed that the total energies of *h*-P₂O₅ and *o'*-P₂O₅ are equal and the total energy of *o'*-P₂O₅ could be used as a surrogate for *h*-P₂O₅. The structural parameters and energies of both phases are given in Table 8 and compared with x-ray measurements (Cruickshank, 1964; Stachel et al. 1995). The calculated electronic energy of *o'*-P₂O₅ is 14.84 kJ/mol lower than *h*-P₂O₅.

Formation of REPO₄ from RE₂O₃ and P₂O₅.

In Table 9 electronic energies at zero temperature [$\Delta E_{\text{e ox}}^{\text{f}}(0) = E_{\text{e}}(\text{REPO}_4) - 1/2(E_{\text{e}}(\text{P}_2\text{O}_5) + E_{\text{e}}(\text{RE}_2\text{O}_3))$] for the reactions:



are tabulated and compared with the measured heats of formation from the oxides at 298.15 K from Ushakov et al. (2002). Figure 1 shows the correlation between $\Delta H_{\text{ox}}^{\text{f}}(298.15)$ and the ionic radius noted by Ushakov et al. (2002), with the cube root of calculated molar volume of the cubic oxide serving as a convenient surrogate for the “computed” value of the ionic radius (this is simpler than, for example, trying to average the calculated RE-O distances). GdPO₄, in the monazite structure deviates most strongly from the correlation. GdPO₄ shows no anomalous predictions in the structural properties of either the RE₂O₃ or REPO₄ phases, and does not deviate strongly in the experimental correlation (Figure 3 in Ushakov et al. (2002)) so the reasons for the large deviation from the energy versus size correlation are not clear, except to note that using the more stable xenotime polymorph for GdPO₄(x) lies much closer to the correlation than GdPO₄(m). There is an indication of a separate, steeper trend for the monazite structures than the xenotime structures. Such a difference was not apparent on the experimental correlation. $\Delta H_{\text{ox}}^{\text{f}}(298.15)$ for TbPO₄(x) and TbPO₄(m) were measured within 3 kJ/mol of each other. This can be compared against the 23 kJ/mol difference in $\Delta E_{\text{e ox}}^{\text{f}}(0)$ for these phases; so it

can be concluded that the DFT calculations overestimate the energetic difference between the two polymorphs.

Figure 2 shows $\Delta H_{\text{ox}}^{\text{f}}(298.15) - \Delta E_{\text{e ox}}^{\text{f}}(0)$ plotted again against the cube root of the volume of the cubic RE_2O_3 phase. The measured $\Delta H_{\text{ox}}^{\text{f}}(298.15)$ values lie fairly consistently about 40 kJ/mol lower than the calculated $\Delta E_{\text{e ox}}^{\text{f}}(0)$, and exhibit no convincing trend with ionic radius, although again, the monazite polymorphs may comprise a trend of increasing $\Delta H_{\text{ox}}^{\text{f}}(298.15) - \Delta E_{\text{e ox}}^{\text{f}}(0)$ with atomic number;. The average deviation would be increased to ~ 50 kJ/mol if *o*'- P_2O_5 were used instead of *h*- P_2O_5 as the P_2O_5 reference compound. The most negative deviations from the average (i.e. the REPO_4 phase is calculated to be thermodynamically less stable than average) occurs for GdPO_4 and TbPO_4 . The most positive deviation is for CePO_4 . Unlike GdPO_4 , calculated structural properties of CePO_4 are anomalous. The predicted volume of CePO_4 is nearly 4.6 percent above x-ray measurements, in contrast to the 2-3 percent for the other REPO_4 . The overestimation of the volume is 4.8 percent for the Ce_2O_3 . Treatment of CePO_4 and Ce_2O_3 with PBE+U makes only a small correction (~ 3 kJ/mol) to the calculated $\Delta E_{\text{e ox}}^{\text{f}}(0)$, so the effective RE_3 pseudopotentials are probably not the source of the error shown in Figure 2. The data in Figure 2 may suggest that the monazite $\text{REPO}_4(\text{m})$ phases lie on a different trend than the xenotime $\text{REPO}_4(\text{x})$ phases. If $\text{LaPO}_4(\text{m})$ is ignored, the difference between calculated and measured heats of formation for the monazite phases fall on a systematic trend with a negative slope (increasing atomic number implies increasingly negative deviation from experiment; in other words, as atomic number increases, the calculated heats of formation become less and less exothermic relative to the measured heats of formation).

Thermal Corrections to $\Delta E_{\text{e ox}}^{\text{f}}(0)$

Direct comparison of the calculated $\Delta E_{\text{e ox}}^{\text{f}}(0)$ for the formation of the REPO_4 from oxides with experimental $\Delta H(298 \text{ K})$ requires, at a minimum, knowledge of the differential zero-point energies $\Delta \text{ZPE} = \text{ZPE}(\text{LnPO}_4) - 1/2[\text{ZPE}(\text{P}_2\text{O}_5) + \text{ZPE}(\text{Ln}_2\text{O}_3)]$ and the differential enthalpies $\Delta \int C_p dT = \int (C_p(\text{LnPO}_4) - 1/2[C_p(\text{Ln}_2\text{O}_3) + C_p(\text{P}_2\text{O}_5)]) dT$ between $(\text{P}_2\text{O}_5 + \text{Ln}_2\text{O}_3)$ and LnPO_4 . These could, in principle, be computed from DFT for all phases, but would require a heavy investment of computational resources. Here, an

empirical approach is taken to estimate the likely magnitude of the thermal contributions. There will also be Schottky-type contributions for some of the phases (Westrum, 1985), but these cannot be responsible for the overall 40 kJ/mol differential between the measured and calculated enthalpies, as they should be close to zero for compounds with no crystal field stabilization (Y, Sc, La, Gd).

The $\Delta \int C_p dT$ can be summed from low-temperature heat capacities of the RE_2O_3 , P_2O_5 , and $REPO_4$ phases. Low-temperature heat capacities for the RE_2O_3 and $REPO_4$ phases (Goldstein et al., 1959; Justice and Westrum, 1963; Weller and King, 1963; Justice et al., 1969; Gavrichev et al., 1993; Gruber et al., 2002) are given in Table 10. Low-temperature heat capacities have been measured for YPO_4 (Gavrichev et al., 2010a), $ScPO_4$ (Gavrichev et al., 2010b), $LaPO_4$ (Gavrichev et al., 2008), and $LuPO_4$ (Gavrichev et al., 2006). The low-temperature heat capacity of P_2O_5 has been measured at 16.98 kJ/mol (Andon et al., 1963); first principles electronic structure calculations yield estimates of $H(298.15) - H(0) = 16.37$ kJ/mol (Rustad, 2011). Taking typical values of ~ 20 kJ/mol for RE_2O_3 , ~ 17 kJ/mol for $REPO_4$, and 16 kJ/mol for P_2O_5 , the thermal enthalpy correction to $\Delta E_{e,ox}^f(0)$ is close to zero (-1 kJ/mol), and cannot account for the systematic difference between $\Delta H(298 K)$ and $\Delta E_{e,ox}^f(0)$.

Estimates for ZPEs can be made empirically from knowledge of the infrared and Raman vibrational spectra for each of the phases. Uncertainties related to the deconvolution of multicomponent peaks, knowledge of vibrational degeneracies, and anharmonic effects contribute to inaccuracies in these estimates. A normal coordinate analysis has been carried for A-type $(La-Pr-Nd)_2O_3$ (Gonipath and Brown, 1982). Infrared and Raman spectra have been measured for $LnPO_4$ ($Ln=La, Ce, Pr, Nd, Sm, Eu, Gd$) (Silva et al., 2006). Infrared and Raman spectra have been obtained for $h-P_4O_{10}$ (Gilliam et al., 2003), however the ZPE for P_2O_5 (70.6 kJ/mol) is taken from a recent theoretical calculation of the vibrational spectrum of this phase (Rustad, 2011) because of some revisions in the interpretation of the measured spectrum indicated by the calculations. The vibrational frequencies and ZPE estimates are given in Tables 11 and 12. Again, taking typical values, an estimate for ΔZPE is $58 \text{ kJ/mol} - \frac{1}{2}(21.5 - 70.6)$. This yields a +12 kJ/mol correction to the calculated $\Delta E_{e,ox}^f(0)$, in the opposite direction of the correction needed to bring the calculated $\Delta E_{e,ox}^f(0)$ in consonance with measured

values of $\Delta H(298\text{ K})$; in other words, the calculated heats become $\sim 12\text{ kJ/mol}$ *less* exothermic by accounting for the ZPE. The calculated heats are already not exothermic enough.

To check these estimates, first principles calculations of the vibrational spectrum of YPO_4 and cubic Y_2O_3 were carried out using the CASTEP planewave-pseudopotential code (Clark et al., 2005), as implemented within Materials Studio of Accelrys, Inc. A plane-wave cutoff of 750 eV and norm-conserving pseudopotentials (Lin et al., 1993; Lee, 1996) were used to do the calculations. The phonons were calculated with the linear-response method (Refson et al., 2006). For Y_2O_3 and YPO_4 the norm-conserving pseudopotentials give structures that compare well with the VASP calculations and experiment (Y_2O_3 : $a=10.594\text{ \AA}$; YPO_4 $a=6.957\text{ \AA}$, $c=5.964\text{ \AA}$) Table 13 gives the thermodynamic properties of Y_2O_3 , YPO_4 , and P_2O_5 . The calculated $\Delta E_{\text{ox}}^{\text{f}}(0)$ is, remarkably, within 1 kJ/mol of the value calculated with VASP. The calculated corrections to obtain $\Delta H_{\text{ox}}^{\text{f}}(298.15)$ from $\Delta E_{\text{ox}}^{\text{f}}(0)$ from both the zero-point energy and the heat capacity are small, on the order of 1 kJ/mol or less. The main discrepancy with the empirical estimate is the calculated ZPE of the oxide. The calculated value for Y_2O_3 (33.5 kJ/mol) is higher than the value estimated from a force field parameterized against the measured vibrational spectra of A-type (La, Pr, Nd) $_2\text{O}_3$ given in Gopinath and Brown (1982). These are, of course, different structures. Calculated frequencies at $q=(0,0,0)$ are given for YPO_4 and Y_2O_3 in Tables 14 and 15, and the phonon density of states for $\text{YPO}_4(x)$ and $c\text{-Y}_2\text{O}_3$ are given in Figures 3 and 4. For $\text{YPO}_4(x)$, there is good agreement between the vibrational frequencies and the Raman spectrum for xenotime reported in (<http://www.ens-lyon.fr/LST/Raman>). For Y_2O_3 there appear to be contributions at significantly higher frequencies than indicated in the measured spectrum (Repelin et al., 1995). It seems reasonable to conclude that the ΔZPE correction probably lies somewhere between 0 and +12 kJ/mol.

Reactivity Trends

The overall trend of increasing $\Delta H_{\text{ox}}^{\text{f}}$ with ionic radius observed by Ushakov et al., (2002) Reference, and reproduced here using electronic structure calculations, is easy

to understand. The electrostatic energies of the oxides and phosphate phases were computed in the ionic model assuming formal charges of +3 for the REE, -2 for oxygen, and +5 for phosphorous. Figure 5 shows the relationship between the electrostatic energy and the ionic radius for the oxide and phosphate phases. To make the comparison easier, the lattice energy of *h*-P₂O₅ has been added to the lattice energy of the oxide phases and the sum is multiplied by 1/2. The difference indicated in the figure is therefore the electrostatic energy of formation (this quantity is highly exothermic because it neglects cation-anion repulsion). The reason for the observed trend is simply that, due to the localized charge on the oxide anions relative to the phosphate anions, the lattice energies of the oxide phases are a stronger function of ionic radius than the phosphates (compare the slopes of 0.82/2 eV/pm for the oxides and 0.34 eV/pm for the phosphates). In other words, the lattice energy becomes more negative for both phases as ionic radius decreases, but does so more rapidly for oxide phase than the phosphate phase because the anionic charge is more localized in the oxide. This type of trend governs the heats of formation of other oxyacid compounds as well, such as sulfates, carbonates, and silicates, as shown in Figure 6, with $\Delta H_{\text{ox}}^{\text{f}}$ taken from the FACTSAGE thermodynamic database.

Conclusions

Density functional electronic structure calculations have been carried out on Sc, Y and RE orthophosphates and oxides, and *h*- and *o*'-P₂O₅ polymorphs to calculate the electronic heats of formation $\Delta E_{\text{ox}}^{\text{f}}(0)$. Calculated heats of formation are systematically approximately 40 kJ/mol less exothermic than measured $\Delta H_{\text{ox}}^{\text{f}}(298.15)$. The systematic error is not uniform with large deviations for Gd(m) (-64.7 kJ/mol) and Ce(m) (-27.6 kJ/mol). For systems where low-temperature heat capacity data are available, H(298.15)-H(0) corrections are estimated to be less than 1 kJ/mol. Empirical estimates for ZPE of orthophosphate and oxide phases are nearly independent of atomic number, and give a 0-+12 kJ/mol correction to the $\Delta E_{\text{ox}}^{\text{f}}(0)$. Ab initio calculation of the zero-point correction for formation of YPO₄, based on the computed vibrational spectrum of YPO₄ and Y₂O₃, gives ΔZPE and $\Delta[\text{H}(298.15)-\text{H}(0)]$ close to zero. Thus the origin of the 40 kJ/mol discrepancy between the measured values of $\Delta H_{\text{ox}}^{\text{f}}(298.15)$ and calculated values of $\Delta E_{\text{ox}}^{\text{f}}(0)$ appears to be electronic in origin. DFT+U calculations for Ce₂O₃ and CePO₄

make only a 3 kJ/mol correction, indicating that the systematic difference cannot be corrected by including electron correlation at the DFT+U level. The observed correlation between atomic number and heat of formation results from the lanthanide contraction and the localized charge on the oxide anion relative to the phosphate anion and can be reproduced from the simplest ionic model.

References

Adelstein, N., Mun, B.S., Ray, H.L., Ross, Jr. P.N., Neaton, J.B., and De Jonghe L.C. (2011) Structure and electronic properties of cerium orthophosphate : Theory and experiment. *Phys. Rev. B.* 83, 205104.

Andon, R.J.L., Counsell, J.F., McKerrell, H., and Martin, J.F. (1963) Thermodynamic properties of phosphorous compounds. 1. Entropy of phosphorous pentoxide. *Trans. Faraday Soc.*, 59, 2702-2705.

Baldinozzi, G., Berar, J., and Calvarin, G. (1998) Rietveld refinement of two-phase Zr-doped Y_2O_3 . *Materials Science Forum*, 278, 680-685.

Bartos, A., Lieb, K.P., Uhrmacher, M., and Wiarda, D. (1993) Refinement of atomic positions in bixbyite oxides using perturbed angular-correlation spectroscopy. *Acta Cryst. B*, 49, 165-169.

Bloch, P.E. (1994) Projector augmented-wave method. *Phys. Rev. B*, 50, 17953.

Boucherle, J.X., and Schweizer, J. (1975) Refinement of Nd_2O_3 structure and determination of neutron-scattering length of neodymium. *Acta Crystallographica B*, 31, 2745-2746.

Boulesteix, C., Pardo, B., Caro, P.E., Gasgnier, M., and la Blanchetais C.H. (1971) Etude de couches minces de sesquioxyde de samarium type B par microscopie et diffraction électroniques. *Acta Crystallographica B*, 27, 216-219.

Clark, S.J., Segall, M.D., Pickard, C.J., Hasnip, P.J., Probert, M.J., Refson K., and Payne M.C. (2005) First-principles methods using CASTEP, *Zeit. Kristallog.*, 220, 567-570.

Cruickshank, D.W.J. (1964) Refinements of structures containing bonds between Si, P, S, or Cl+O or N V. P_4O_{10} . *Acta Cryst.*, 17, 677-679.

Da Silva, J.L. (2007) Stability of the Ce_2O_3 phases: a DFT+U investigation. *Phys. Rev. B*, 76, 193108.

Dudarev, S.L., Botton, G.A., Savrasov, S.Y., Szotek, Y., Temmerman, W.M., and Sutton A.P. (1998) Electronic structure and elastic properties of strongly correlated metal oxides from first principles: LSDA+U, SIC-LSDA and EELS study of UO_2 and NiO. *Phys. Status Solidi A*, 166, 429-443.

Fabris, S., de Gironcoli, S., Baroni, S., Vicario, G., and Balducci G. (2005) Taming multiple valency with density functionals: A case of defective ceria. *Phys. Rev. B*, 71, 041102.

Fert, A.(1962) Structure de quelques oxydes de terres rares. *Bulletin de la Societe Francaise de Mineralogie et de Cristallographie*, 85, 267-270.

Gavrichev, K.S., Gorbunov, V.E., Golushina, L.N., Nikiforova, G.E., Totrova, G.A., and Shaplygin, I.S. (1993) Calorimetry and thermodynamic properties of Y_2O_3 in 14-300 K temperature range. *Zhurnal Fizichyeskoi Khimi*, 67, 1731-1733.

Gavrichev, K.S., Smirnova, N.N., Gurevich, V.M., Danilov, V.P., Tyurin, A.V., Ryumin, M.A., and Komissarova, L.N. (2006) Heat capacity and thermodynamic functions of $LuPO_4$ in the range 0-320 K. *Thermochimica Acta*, 448, 63-65.

Gavrichev, K.S., Ryumin, M.A., Tyurin, A.V., Gurevich, V.M., and Komissarova, L.N. (2008) Refined heat capacity of $LaPO_4$ in the temperature range 0-1600 K. *Thermochimica Acta*, 474, 47-51.

Gavrichev, K.S., Ryumin, M.A., Tyurin, A.V., Gurevich, V.M., and Komissarova, L.N. (2010a) Heat capacity and thermodynamic functions of pretulite $ScPO_4(c)$ at 0-1600 K. *Geochim. International*, 48, 390-397.

Gavrichev, K.S., Ryumin, M.A., Tyurin, A.V., Gurevich, V.M., and Komissarova, L.N. (2010b) Heat capacity and thermodynamic functions of xenotime $YPO_4(c)$ at 0-1600 K. *Geochim. International*, 48, 932-939.

Gilliam, S.J., Kirby, S.J., Merrow, C.N., Zeroka, D., Banerjee, A., and Jensen, J.O. (2003) Raman spectroscopy of rhombohedral P_4O_{10} . *J. Phys. Chem. B*, 107, 2892-2896.

Goldstein, H.W., Neilson, E.F., Walsh, P.N., and White D. (1959) The heat capacities of yttrium oxide (Y_2O_3), lanthanum oxide (La_2O_3), and neodymium oxide (Nd_2O_3) from 16 to 300 degrees K. *J. Phys. Chem.*, 63, 1445-1449.

Gopinath, C.R., and Brown, I.D. (1982) Normal coordinate analysis of the Raman and infrared vibrations of the alpha phases of La_2O_3 , Pr_2O_3 , Nd_2O_3 , $\text{La}_2\text{O}_2\text{S}$, $\text{YB}_2\text{O}_2\text{S}$. *J. Raman Spectroscopy*, 12, 278-280.

Greenwood, N.N., Earnshaw A. *Chemistry of the Elements*, Butterworth Heinemann, Oxford, 1985.

Greis, O., Ziel, R., Breidenstein, B., Haase, A., and Petzel, T. (1994) The crystal-structure of the low-temperature A-type modification of Pr_2O_3 from X-ray powder and electron single crystal diffraction. *J. Alloys Compd.*, 216, 255-258.

Gruber, J.B., Justice, B.H., Westrum, E.F., Zandi, B. (2002) Revisiting the thermophysical properties of the A-type hexagonal lanthanide sesquioxides between temperatures of 5 K and 1000 K. *J. Chem. Thermodynamics*, 34, 457-473.

Gurmani, S., Jahn, S., Brasse, H., Schilling, F.R. (2010): Does a Dielectric Double Layer Evolve in Partially Molten Rocks? American Geophysical Union Fall Meeting (San Francisco, USA).

Hase, W. (1963) Neutronographische bestimmung der kristallstrukturparameter von Dy_2O_3 , Tm_2O_3 , und alpha- Mn_2O_3 , *Physica Status Solidi*, 3, 446-449.

Hirosaki, N., Ogata, S., and Kocer, C.J. (2003) Ab initio calculation of the crystal structure of the lanthanide Ln_2O_3 sesquioxides. *Alloys and Compounds*, 351, 31-34.

Justice, B.H., and Westrum, E.F. (1963a) Thermophysical properties of the lanthanide oxides. 2. Heat capacities, thermodynamic properties and some energy levels of

samarium(III), gadolinium(III), and ytterbium(III) oxides from 10 to 350 degrees K. J. Phys. Chem., 67, 345-351.

Justice, B.H., Westrum, E.F., Chang, E., and Radebaug, R. (1969) Thermophysical properties of the lanthanide oxides. 4. Heat capacities and thermodynamic of thulium(III) and lutetium(III) oxides. Electronic energy levels of several lanthanide (III) ions. J. Phys. Chem., 73, 333-340.

Knop, O., and Hartley, J.M. (1968) Refinement of the crystal structure of scandium oxide Can. J. Chem.. 46, 1446-1450.

Koehler, W.C., and Wollan, E.O. (1953) Neutron-diffraction study of the structure of the A-form of the rare earth sesquioxides Acta Cryst., 6, 741-742.

Kresse, G., and Furthmuller, J. (1996) Efficiency of ab-initio total energy calculations for metals and semiconductors using a plane-wave basis set. Comput. Mater. Sci., 6, 15-50.

Kresse, G., and Hafner, J. (1993) Ab initio molecular dynamics for liquid-metals Phys. Rev. B, 47, 558-561.

Kresse, G., Joubert, D. (1999) From ultrasoft pseudopotentials to the projector augmented-wave method Phys. Rev. B, 59, 1758-1775.

Kuemmerle, E.A., Heger, G.J. (1999) The structures of C-Ce₂O₃+delta, Ce₇O₁₂, and Ce₁₁O₂₀, Solid State Chem., 147, 485-500.

Lin, J.S., Qteish, A., Payne, M.C., and Heine, V. (1993) Optimized and transferable nonlocal separable ab initio pseudopotentials, Phys. Rev. B, 47, 4174-4180.

Loschen, C., Carrasco, J., Neyman, K.M., and Illas, F. (2007) First-principles LDA plus U and GGA plus U study of cerium oxides: Dependence on the effective U parameter Phys. Rev. B., 75, 035115.

Milligan, W.O., Mullica, D.F., Beall, G.W., and Boatner, L.A. (1982) Structural investigations of YPO_4 , ScPO_4 , and LuPO_4 Inorganica Chimica Acta, 60, 39-43.

Ni, Y., Hughes, J.M., and Mariano, A.N. (1995) Crystal chemistry of the monazite and xenotime structures Am. Mineralogist, 80, 21-26.

Pedone, A., Malavasi, G., Menziani, M.C., Cormack, A.N., and Segre, U. (2006) A new self-consistent empirical interatomic potential model for oxides, silicates, and silica-based glasses. J. Phys. Chem. B, 110, 11780-11795.

Perdew, J.P., Burke, K., and Ernzerhof, M. (1996) Generalized gradient approximation made simple Phys. Rev. Lett., 77, 3865-3868.

Refson, K., Clark, S.J., and Tulip, P.R. (2006) Variational density-functional perturbation theory for dielectrics and lattice dynamics Phys. Rev. B, 73, 155114.

Repelin, Y., Proust, C., Husson, E., and Beny, J.M. (1995) Vibrational spectroscopy of the C-form of yttrium sesquioxide. J. Solid State Chem., 118, 163-169.

Rustad, J.R. (2011) Vibrational Spectrum and Low-Temperature Heat Capacity of Rhombohedral P_4O_{10} arXiv:1106.5824v1[cond-mat.mtrl-sci]

Saiki, A., Ishizawa, N., Mizutani, N., and Kato, M. (1985) Structural change of rare earth sesquioxides Yb_2O_3 and Er_2O_3 as a function of temperature. *J. Ceram. Soc. Japan*, 93, 649-654.

Schiller, G., Die Kristallstrukturen von Ce_2O_3 (A-Form), LiCeO_2 und CeF_3 - Ein Beitrag zur Kristallchemie des dreiwertigen Cers, Dissertation Universitaet Karlsruhe 1985.

Silva, E.N., Ayala, A.P., Guedes, I., Paschoal, C.W.A., Moriera, R.L., Loong, C.-K., and Boatner, L (2006) Vibrational spectra of monazite-type rare-earth orthophosphates. *Optical Materials*, 29, 224-230.

Stachel, D., Svoboda, I., and Fuess, H. (1995) Phosphorous pentoxide at 233 K. *Acta Cryst. C*, 51, 1049-1050.

Ushakov, S.V., Helean, K.B., and Navrotsky, A. (2002) Thermochemistry of rare-earth orthophosphates. *J. Mater. Res.*, 16, 2623-2633.

Weller, W.W., and King, E.G. (1963) Report Invest No 6245 US Bureau of Mines p. 1-6

Westrum, E.F., and Justice, B.H. (1963) Thermophysical properties of the lanthanide oxides. 2. Heat capacities, thermodynamic properties and some energy levels of dysprosium(III), holmium(III), and erbium(III) oxides. *J. Phys. Chem.*, 67, 659-665.

Westrum, E. F. (1985) Schottky contributions in chemical thermodynamics. *Journal of Thermal Analysis and Calorimetry*, 30, 1209-1215.

Wu, B., Zinkevich, M., Aldinger, F., Wen, D., and Chen, L. (2007) Ab initio study on the structure and phase transition of A- and B-type rare-earth sesquioxides Ln_2O_3 (Ln=La-Lu, Y, and Sc) based on density functional theory. *J. Solid State Chem.*, 180, 3280-3287.

Zhang, F.X., Lang, M., Wang, J.W., Becker, U., and Ewing, R.C. (2008) Structural phase transitions of cubic Gd_2O_3 at high pressures, *Physical Review B*, 78, 064114.

Figure Captions

Figure 1. Correlation between $\Delta E_{e_{ox}}^f(0)$ and the cube root of the computed volume of the RE_2O_3 phase. (m) monazite, (x) xenotime.

Figure 2. Correlation between the difference of the measured heat of formation and the computed electronic energy [$\Delta H_{ox}^f(298.15) - \Delta E_{e_{ox}}^f(0)$] and the cube root of the computed volume of the cubic RE_2O_3 .

Figure 3. Phonon density of states computed for YPO_4 -xenotime.

Figure 4. Phonon density of states computed for cubic Y_2O_3 .

Figure 5. Electrostatic lattice energies E as a function of ionic radius for RE oxide and phosphate phases. The lattice energy of h - P_2O_5 has been added to the oxides and the sum multiplied by $1/2$.

Figure 6. Correlation between heat of formation from the oxides and ionic radius for carbonate (MO_3), orthosilicate (M_2SiO_4), and sulfate(MSO_4) compounds with divalent anions. Data taken from FACTSAGE thermodynamic database.

Table 1. Structural Parameters for hexagonal A-type RE₂O₃ (volumes in Å³/formula unit)

	Calculated									Measured		
	This work			Hirosaki et al., (2003)			Wu et al. (2007)			a (Å)	c (Å)	V(Å ³)
	a (Å)	c (Å)	V(Å ³)	a (Å)	c (Å)	V(Å ³)	a (Å)	c (Å)	V(Å ³)	a (Å)	c (Å)	V(Å ³)
La ₂ O ₃ ^a	3.936	6.200	83.20	3.936	6.166	82.73	3.938	6.173	82.90	3.940	6.13	82.410
Ce ₂ O ₃ ^b	3.944	6.180	83.26	3.941	6.182	83.14	3.944	6.191	83.38	3.891	6.059	79.440
Ce ₂ O ₃ (PBE+U) AFM	3.897	6.229	81.91									
Ce ₂ O ₃ (PBE+U) FM	3.892	6.224	81.66									
Pr ₂ O ₃ ^c	3.896	6.135	80.64	3.895	6.126	80.50	3.899	6.135	80.76	3.859	6.0131	77.550
Nd ₂ O ₃ ^d	3.867	6.082	78.77	3.859	6.072	78.30	3.859	6.090	78.54	3.831	5.999	76.250

^aKoehler and Wollan, 1953; ^bSchiller, 1985; ^cHase, 1963; ^dBoucherle and Schweizer, 1975

Table 2. Structural Parameters for monoclinic B-type RE₂O₃ (volume in Å³/formula unit)

	a (Å)	b (Å)	c (Å)	β	V(Å ³)
calc (this work)					
Sm ₂ O ₃	14.384	3.631	8.916	100.26	76.36
Gd ₂ O ₃	14.177	3.565	8.770	100.30	72.68
calc ^a					
Sm ₂ O ₃	14.381	3.635	8.911	100.15	76.41
Gd ₂ O ₃	14.195	3.566	8.770	100.18	72.80
measured					
Sm ₂ O ₃ ^b	14.198	3.627	8.856	99.99	74.66
Gd ₂ O ₃ ^c	14.032	3.583	8.742	100.13	72.11

^aWu et al., 2007; ^bBoulestix et al, 1971; ^cZhang et al., 2008

Table 3. Structural Parameters for cubic C-type RE₂O₃ (volume in Å³/formula unit)

	calculated		measured			
	This work		Hirosaki et al., (2003)		a (Å)	V(Å ³)
	a (Å)	V(Å ³)	a (Å)	V(Å ³)		
Sc ₂ O ₃	9.911	60.85			9.846 ^a	59.66
Y ₂ O ₃	10.701	76.58			10.596 ^b	74.36
La ₂ O ₃	11.387	92.29	11.392	92.40		
Ce ₂ O ₃	11.414	92.94	11.410	92.84	11.111 ^c	85.73
Pr ₂ O ₃	11.290	89.94	11.288	89.89		
Nd ₂ O ₃	11.178	87.30	11.176	87.24		
Sm ₂ O ₃	10.998	83.14	10.995	83.07	10.930 ^d	81.61
Gd ₂ O ₃	10.819	79.16	10.812	78.99	10.790 ^d	78.51
Tb ₂ O ₃	10.744	77.50			10.729 ^e	77.10
Dy ₂ O ₃	10.675	76.02	10.670	75.92	10.670 ^d	75.92
Ho ₂ O ₃	10.609	74.63	10.605	74.54	10.580 ^d	74.02
Er ₂ O ₃	10.544	73.26	10.544	73.26	10.548 ^f	73.35
Tm ₂ O ₃	10.472	71.77			10.480 ^g	71.94

^aKnop and Hartley, 1963; ^bBaldinozzi et al., 1998; ^cKuemmerle and Heger, 1999; ^dBartos et al., 1993;

^eSaiki et al., 1985; ^fFert, 1962; ^gHase, 1963

Table 4. Energies of RE₂O₃ phases (eV/formula unit).

	C-type	A-type	B-type	A-type ^a	B-type ^a
Sc ₂ O ₃	-45.2887			-44.6351	-44.9478
Y ₂ O ₃	-45.5652			-45.2299	-45.3291
La ₂ O ₃	-42.0219	-41.9007		-41.9079	-41.8576
Ce ₂ O ₃	-40.7455	-40.6337		-40.6376	-40.6027
Ce ₂ O ₃ (PBE+U) AFM		-41.6814			
Ce ₂ O ₃ (PBE+U) FM		-41.6791			
Pr ₂ O ₃	-41.0188	-40.8856		-40.8945	-40.8744
Nd ₂ O ₃	-41.2258	-41.0714		-41.0803	-41.0746
Sm ₂ O ₃	-41.5301		-41.3677	-41.3363	-41.362
Gd ₂ O ₃	-41.8636		-41.6746	-41.6172	-41.6718
Tb ₂ O ₃	-41.9675			-41.7017	-41.7655
Dy ₂ O ₃	-42.0428			-41.7398	-41.8283
Ho ₂ O ₃	-42.1142			-41.8004	-41.8883
Er ₂ O ₃	-42.2007			-41.8377	-41.9627
Tm ₂ O ₃	-42.1943			-41.7963	-41.9437

^aWu et al., 2007

Table 5. Structural parameters for REPO₄ in the xenotime (zircon) structure (volume in Å³/formula unit)

	calculated			measured		
	a (Å)	c (Å)	V (Å ³)	a (Å)	c (Å)	V (Å ³)
ScPO ₄ ^a	6.661	5.837	64.740	6.574	5.791	62.568
YPO ₄ ^a	6.976	6.079	73.950	6.895	6.028	71.633
TbPO ₄ ^b	6.984	6.086	74.205	6.931	6.061	72.784
DyPO ₄ ^b	6.953	6.066	73.328	6.905	6.038	71.981
HoPO ₄ ^b	6.934	6.050	72.710	6.877	6.018	71.154
ErPO ₄ ^b	6.905	6.026	71.823	6.851	5.997	70.363
TmPO ₄ ^b	6.880	5.998	70.968	6.829	5.980	69.726
LaPO ₄	7.274	6.347	83.945			
CePO ₄	7.261	6.342	83.575			
CePO ₄ (PBE+U ^c)	7.233	6.314	82.62			
PrPO ₄	7.209	6.293	81.768			
NdPO ₄	7.178	6.247	80.473			
SmPO ₄	7.089	6.187	77.728			
GdPO ₄	7.015	6.116	75.248			

^aMilligan et al, 1982; ^bNi et al., 1995; ^cferromagnetic electronic state

Table 6. Structural parameters for REPO₄ in the monazite structure. (volume in Å³/formula unit)

	calculated					measured ^a				
	a (Å)	b(Å)	c(Å)	β (deg)	V(Å ³)	a (Å)	b(Å)	c(Å)	β (deg)	V(Å ³)
LaPO ₄	6.932	7.142	6.543	103.6	78.71	6.831	7.071	6.503	103.3	76.43
CePO ₄	6.916	7.135	6.535	103.5	78.40	6.788	7.016	6.465	103.4	74.98
AFM1 ^b	6.900	7.110	6.510	103.5	77.62					
AFM2	6.883	7.099	6.522	103.6	77.44					
AFM3	6.908	7.113	6.515	103.5	77.82					
FM ^c	6.899	7.105	6.518	103.6	77.64					
PrPO ₄	6.873	7.079	6.485	103.8	76.61	6.760	6.981	6.434	103.5	73.80
NdPO ₄	6.840	7.040	6.452	103.8	75.42	6.735	6.950	6.405	103.7	72.83
SmPO ₄	6.803	6.961	6.394	104.2	73.38	6.682	6.888	6.365	103.9	71.10
GdPO ₄	6.713	6.887	6.358	104.2	71.24	6.644	6.841	6.328	104.0	69.78
TbPO ₄	6.687	6.858	6.337	104.2	70.42					

^aNi et al., 1995; ^bantiferromagnetic electronic states; ^cferromagnetic electronic state

Table 7. Calculated Energies of REPO₄ (eV/formula unit).

	x-type	m-type
ScPO ₄ (x)	-48.845	
YPO ₄ (x)	-49.760	
LaPO ₄ (m)	-48.215	-48.337
CePO ₄ (m)	-47.679	-47.805
CePO ₄ (PBE+U) AFM1		-48.280
CePO ₄ (PBE+U) AFM2		-48.304
CePO ₄ (PBE+U) AFM3		-48.251
CePO ₄ (PBE+U) FM	-47.970	-48.302
PrPO ₄ (m)	-47.779	-47.843
NdPO ₄ (m)	-47.846	-47.854
SmPO ₄ (m)	-47.923	-47.835
GdPO ₄ (m)	-48.013	-47.819
TbPO ₄ (x)	-48.027	-47.788
DyPO ₄ (x)	-48.025	
HoPO ₄ (x)	-48.022	
ErPO ₄ (x)	-48.031	
TmPO ₄ (x)	-47.991	

Table 8. Structural parameters and energies of P₂O₅ phases.

	(a,b,c)(Å)	(a,b,g) deg		V(Å ³)	E (eV/formula unit)
h-P ₂ O ₅	7.592	87.6		109.1	-48.9743
measured ^a	7.43	87		102.1	
	a(Å)	b(Å)	c(Å)		
o'-P ₂ O ₅	9.534	4.952	7.308	345.0	-49.1281
measured ^b	9.139	4.89	7.162	320.1	

^aCruickshank, 1964

^bStachel et al., 1995

Table 9. Measured vs. calculated electronic energy (kJ/mol)

	$\Delta H_{\text{ox}}^{\text{f}}(298.15)$ kJ/mol ^a	$\Delta E_{\text{ox}}^{\text{f}}(0)$ kJ/mol	$\Delta H_{\text{ox}}^{\text{f}}(298.15) - \Delta E_{\text{ox}}^{\text{f}}(0)$ kJ/mol
YPO ₄ (x)	-282.6	-240.2	-42.4
LaPO ₄ (m)	-321.4	-279.7	-41.7
LaPO ₄ (x)		-268.0	-53.4
CePO ₄ (m)	-317.2	-289.6	-27.6
PBE+U AFM1		-287.1	-30.1
PBE+U AFM2		-284.8	-32.4
PBE+U AFM3		-282.0	-35.2
PBE+U FM		-287.0	-30.2
CePO ₄ (x)		-277.4	-39.8
PrPO ₄ (m)	-312.2	-281.1	-31.1
PrPO ₄ (x)		-274.8	-37.4
NdPO ₄ (m)	-312.0	-273.2	-38.8
NdPO ₄ (x)		-272.3	-39.7
SmPO ₄ (m)	-301.8	-257.1	-44.7
SmPO ₄ (x)		-265.5	-36.3
GdPO ₄ (m)	-296.2	-231.6	-64.6
GdPO ₄ (x)		-250.3	-45.9
TbPO ₄ (x)	-286.1	-246.6	-39.5
TbPO ₄ (m)	-283.5	-223.5	-60.0
DyPO ₄ (x)	-283.9	-242.8	-41.1
HoPO ₄ (x)	-278.8	-239.1	-39.7
ErPO ₄ (x)	-275.6	-235.7	-39.9
TmPO ₄ (x)	-268.0	-232.2	-35.8
ScPO ₄ (x)	-209.8	-165.4	-44.4

^aUshakov et al., 2002

Table 10. Enthalpy correction to standard temperature H(298.15)-H(0) for RE₂O₃ phases (kJ/mol)

	RE ₂ O ₃	REPO ₄
Sc	13.845 ^a	14.934 ^g
Y	16.800 ^b	15.944 ^h
La	19.842 ^c	17.440 ⁱ
Ce	21.479 ^c	
Pr	22.734 ^c	
Nd	20.892 ^c	
Sm	21.008 ^d	
Gd	18.510 ^d	
Dy	21.025 ^e	
Ho	20.958 ^e	
Er	19.995 ^e	
Tm	20.887 ^f	
Lu	17.539 ^f	16.430 ^j

^aWeller and King, 1963; ^bGavrichev et al., 1993; ^cGruber et al., 2002; ^dJustice and Westrum, 1963; ^eWestrum and Justice, 1963; ^fJustice et al., 1969; ^gGavrichev et al, 2010a; ^hGavrichev et al., 2010b; ⁱGavrichev et al. 2008; ^jGavrichev et al., 2006

Table 11. Vibrational frequencies (cm^{-1}) with $h\nu/2$ contribution to zero point energy (kJ/mol) for monazite-type LnPO_4 .^a

LaPO_4		CePO_4		PrPO_4		NdPO_4		SmPO_4		EuPO_4		GdPO_4	
90	0.5	88	0.5	90	0.5	89	0.5	88	0.5	87	0.5	87	0.5
100	0.6	100	0.6	105	0.6	106	0.6	107	0.6	108	0.6	108	0.6
151	0.9	152	0.9	153	0.9	154	0.9	155	0.9	156	0.9	158	0.9
157	0.9	158	0.9	160	1.0	160	1.0	159	1.0	160	1.0	162	1.0
170	1.0	172	1.0	176	1.1	175	1.0	177	1.1	175	1.0	178	1.1
184	1.1	183	1.1	182	1.1	183	1.1	185	1.1	189	1.1	192	1.1
219	1.3	219	1.3	225	1.3	228	1.4	231	1.4	234	1.4	236	1.4
226	1.4	227	1.4	233	1.4	236	1.4	243	1.5	243	1.5	247	1.5
258	1.5	254	1.5	260	1.6	264	1.6	265	1.6	265	1.6	268	1.6
275	3.3	270	1.6	282	1.7	291	1.7	293	1.8	298	1.8	302	1.8
396	2.4	396	2.4	299	1.8	398	2.4	404	2.4	404	2.4	406	2.4
413	2.5	414	2.5	417	5.0	419	2.5	424	2.5	425	2.5	428	2.6
466 ^b	5.6	467	5.6	470	5.6	471	5.6	474	5.7	472	5.6	478	5.7
620 ^c	11.1	618	11.1	623	11.2	625	11.2	629	11.3	631	11.3	634	11.4
968 ^d	5.8	970	5.8	975	5.8	977	5.8	983	5.9	990	5.9	988	5.9
1054 ^e	18.9	1054	18.9	1058	19.0	1061	19.0	1065	19.1	1069	19.2	1072	19.2
	58.8 ^f		57.1 ^f		59.6 ^f		57.9 ^f		58.3 ^f		58.5 ^f		58.8 ^f

^adata taken from Silva et al., 2006.

^b $\text{PO}_4\text{-v}_2$ (multiplicity 2), ^c $\text{PO}_4\text{-v}_4$ (multiplicity 3), ^d $\text{PO}_4\text{-v}_1$ (multiplicity 1), ^e $\text{PO}_4\text{-v}_3$ (multiplicity 3),

^f total zero-point energy ($\sum h\nu_i/2$)

Table 12. Vibrational frequencies (cm^{-1}) with $h\nu/2$ contribution to zero point energy (kJ/mol) for A-type Ln_2O_3 oxide phases.^a

	La_2O_3		Pr_2O_3		Nd_2O_3	
E_g	413	4.9	415	5.0	434	5.2
A_{1g}	400	2.4	404	2.4	422	2.5
E_u	408	4.9	409	4.9	415	5.0
A_{2a}	404	2.4	406	2.4	407	2.4
E_u	243	2.9	264	3.2	232	2.8
A_{2u}	256	1.5	258	1.5	223	1.3
A_{1g}	191	1.1	189	1.1	190	1.1
E_g	99	1.2	99	1.2	100	1.2
		21.4 ^b		21.7 ^b		21.6 ^b

^adata taken from Gopinath and Brown, 1982.

^btotal zero-point energy ($\sum h\nu_i/2$)

Table 13. Thermodynamic properties obtained with CASTEP

	E_e	ZPE [kJ mol^{-1}]	C_v [$\text{J mol}^{-1} \text{K}^{-1}$]	H(298.15)- H(0) [kJ mol^{-1}]	S(298.15) [$\text{J K}^{-1} \text{mol}^{-1}$]
YPO_4 calc (this work)	-1957.54 eV	53.14	96.84 $\text{J mol}^{-1} \text{K}^{-1}$ (C_v)	15.001	87.28
exp ^a		-	99.27 $\text{J mol}^{-1} \text{K}^{-1}$ (C_p)	15.994	93.86
Y_2O_3 calc (this work)	-1393.97 eV	33.45	93.66	14.760	85.92
exp ^b		-	103.4	16.800	98.96
$h\text{-P}_2\text{O}_5$ calc ^c	-2516.15 eV	70.65	103.1 $\text{J K}^{-1} \text{mol}^{-1}$	16.370	106.45
$\Delta E_{e\text{ox}}^f(0)$	-239.28 kJ/mol				
Correction to H calc		1.09		-0.56	
exp ^d	-282.6 kJ/mol			-0.59	

^aGavrichev et al., 2010; ^bGavrichev et al., 1993; ^cRustad, 2011; ^dUshakov et al., 2002.

Table 14. Computed vibrational modes at $q=(0,0,0)$ for Y_2O_3

$\nu(\text{cm}^{-1})$	g^a	IR Int ^b	IR ^c	RM ^b						
114.4	1	0.00	N	N	412.5	3	51.24	Y	N	
122.0	3	0.04	Y	N	419.7	1	0.00	N	Y	
132.1	3	0.00	N	Y	420.6	2	0.00	N	N	
135.7	2	0.00	N	N	425.5	3	1.70	Y	N	
141.1	3	0.00	N	Y	435.1	3	0.00	N	Y	
159.0	3	0.01	Y	N	448.6	3	100.11	Y	N	
166.6	1	0.00	N	Y	452.3	3	0.00	N	Y	
177.2	3	0.23	Y	N	463.4	2	0.00	N	Y	
187.5	3	0.17	Y	N	470.6	2	0.00	N	N	
193.0	3	0.00	N	Y	471.6	3	0.00	N	Y	
207.1	2	0.00	N	Y	476.5	3	3.71	Y	N	
207.9	3	0.06	Y	N	506.0	1	0.00	N	Y	
241.7	1	0.00	N	N	514.7	3	0.00	N	Y	
253.2	3	0.00	N	Y	518.5	1	0.00	N	N	
257.3	3	0.00	N	Y	551.8	3	4.12	Y	N	
260.7	2	0.00	N	N	556.5	3	0.00	N	Y	
261.6	3	1.08	Y	N	580.4	1	0.00	N	N	
320.2	3	0.00	Y	N	581.4	3	0.02	Y	N	
378.6	3	88.12	Y	N	593.1	3	0.00	N	Y	
385.1	3	0.00	N	Y	624.0	3	18.35	Y	N	
393.5	3	2.04	Y	N	633.5	1	0.00	N	Y	
394.9	1	0.00	N	N	635.5	2	0.00	N	Y	
397.1	2	0.00	N	Y	653.4	2	0.00	N	N	
398.5	3	0.00	N	Y	663.8	3	0.00	N	Y	

^adegeneracy; ^binfrared intensity
($\text{debye}^2/\text{\AA}^2/\text{atomic mass unit}$), ^cinfrared
active, ^draman active

Table 15. Computed vibrational modes at $q=(0,0,0)$ for YPO_4

$\nu(\text{cm}^{-1})$	g^a	IR Int ^b	IR ^c	RM ^b
154.2	1	0.0	N	N
166.4	2	0.0	N	Y
190.3	1	0.0	N	Y
236.6	2	0.0	N	Y
237.7	2	10.1	Y	N
244.0	1	0.0	N	N
324.6	2	0.0	N	Y
339.2	1	0.0	N	Y
351.9	1	29.9	Y	N
352.9	1	0.0	N	Y
381.8	2	2.3	Y	N
418.0	1	0.0	N	N
518.9	1	0.0	N	Y
526.3	2	4.0	Y	N
577.5	1	0.0	N	N
584.8	2	0.0	N	Y
647.8	1	11.4	Y	N
669.2	1	0.0	N	Y
954.6	2	48.2	Y	N
957.6	1	0.0	N	N
971.7	1	0.0	N	Y
995.8	2	0.0	N	Y
1023.3	1	0.0	N	Y
1024.8	1	53.4	Y	N

^adegeneracy; ^binfrared intensity ($\text{debye}^2/\text{\AA}^2/\text{atomic mass unit}$), ^cinfrared active, ^draman active

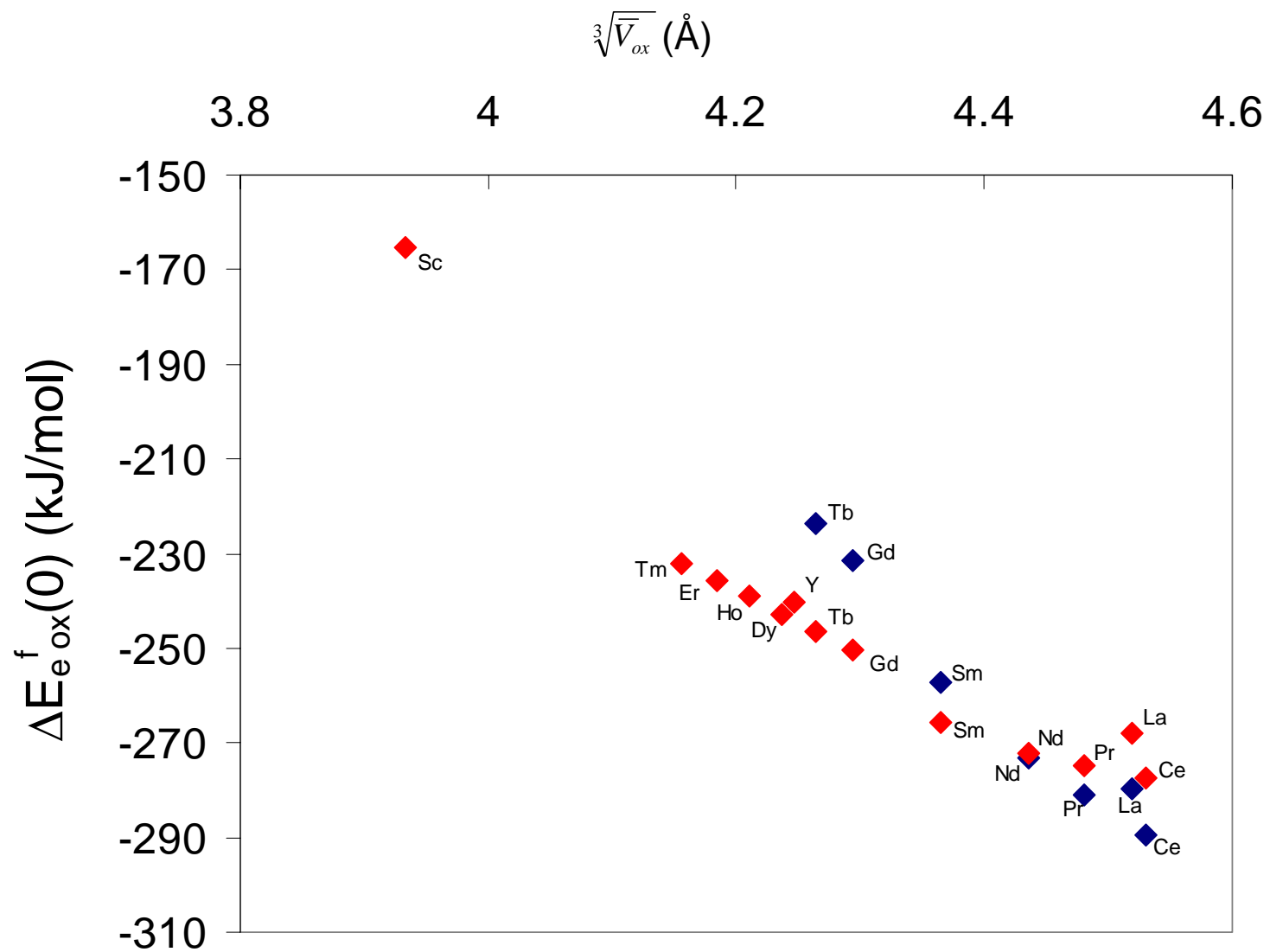


Figure 1. Correlation between $\Delta E_{e_{ox}}^f(0)$ and the cube root of the computed volume of the RE_2O_3 phase. (m) monazite, (x) xenotime

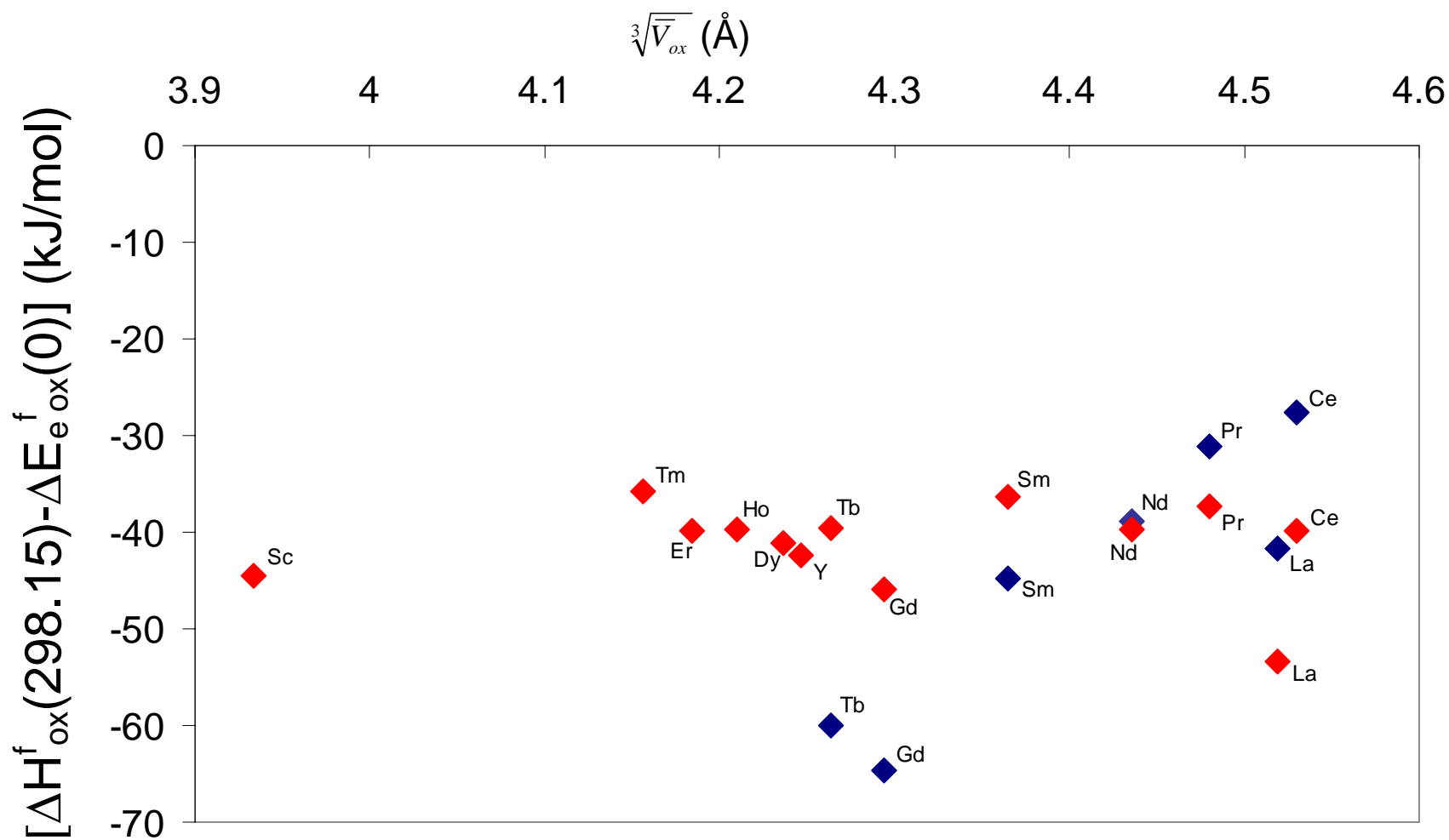


Figure 2. Correlation between the difference of the measured heat of formation and the computed electronic energy $[\Delta H_{ox}^f(298.15) - \Delta E_{e_{ox}}^f(0)]$ and the cube root of the computed volume of the cubic RE_2O_3 .

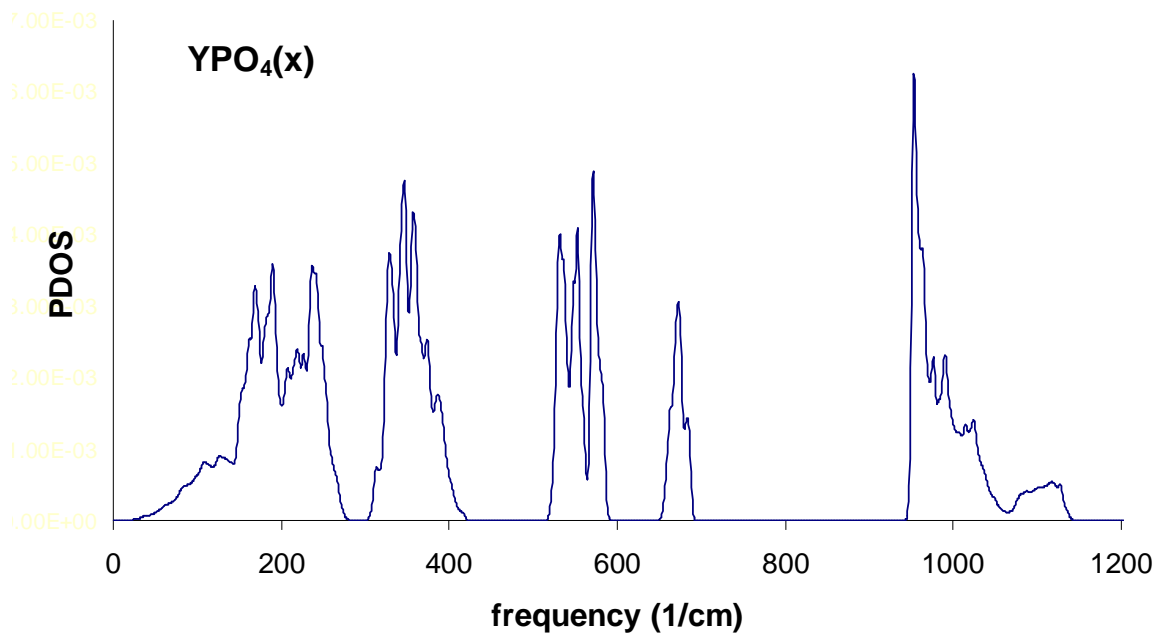


Figure 3. Phonon density of states computed for YPO₄-xenotime.

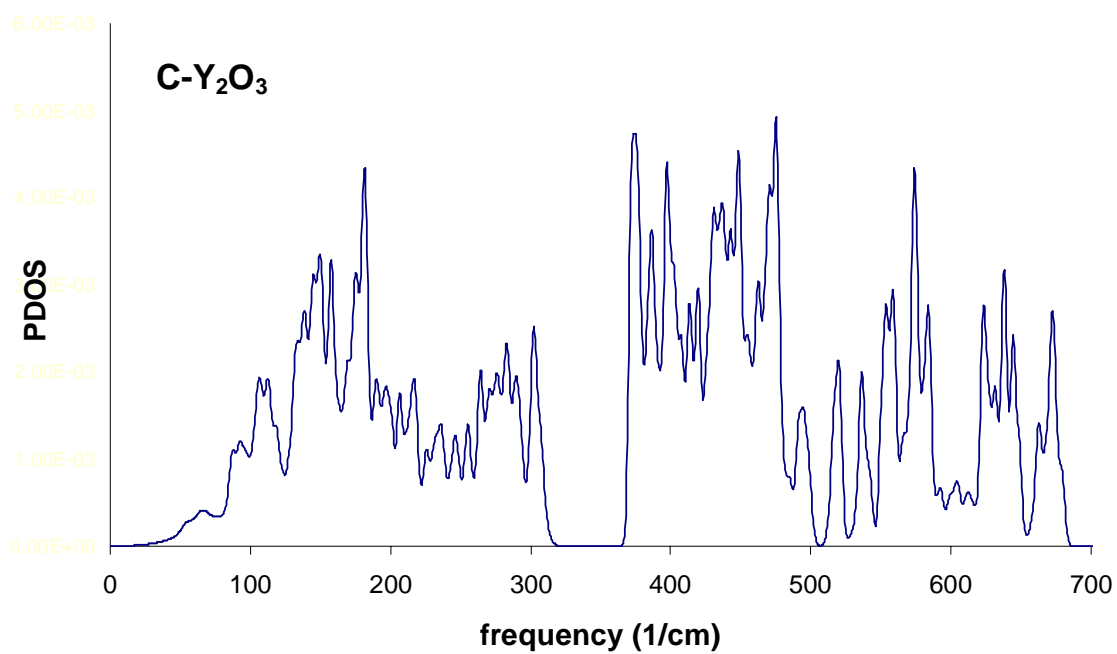


Figure 4. Phonon density of states computed for cubic Y_2O_3 .

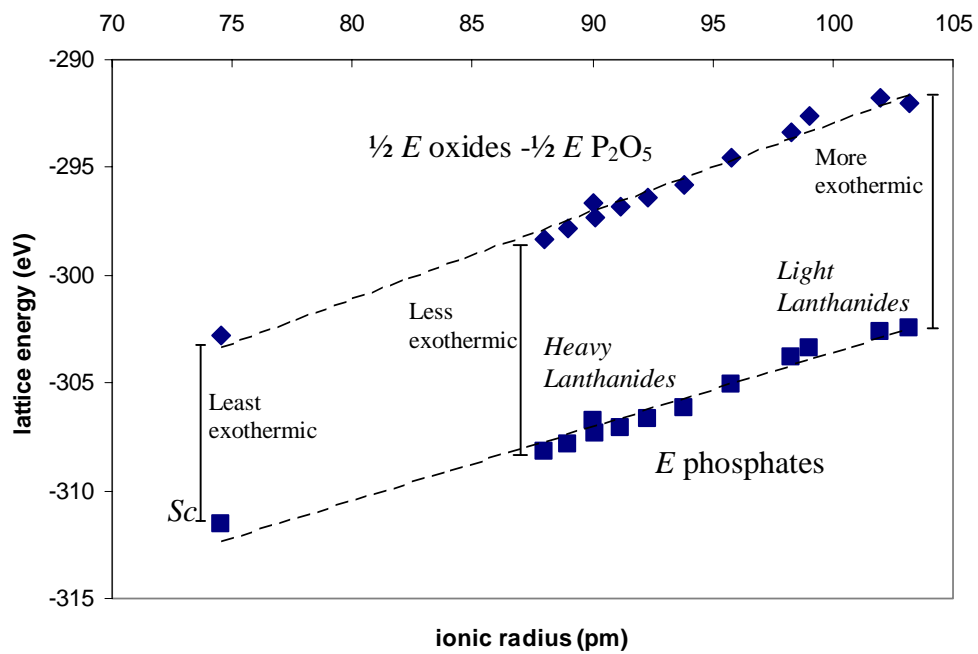


Figure 5. Electrostatic lattice energies E as a function of ionic radius for RE oxide and phosphate phases. The lattice energy of $h\text{-P}_2\text{O}_5$ has been added to the oxides and the sum multiplied by $\frac{1}{2}$.

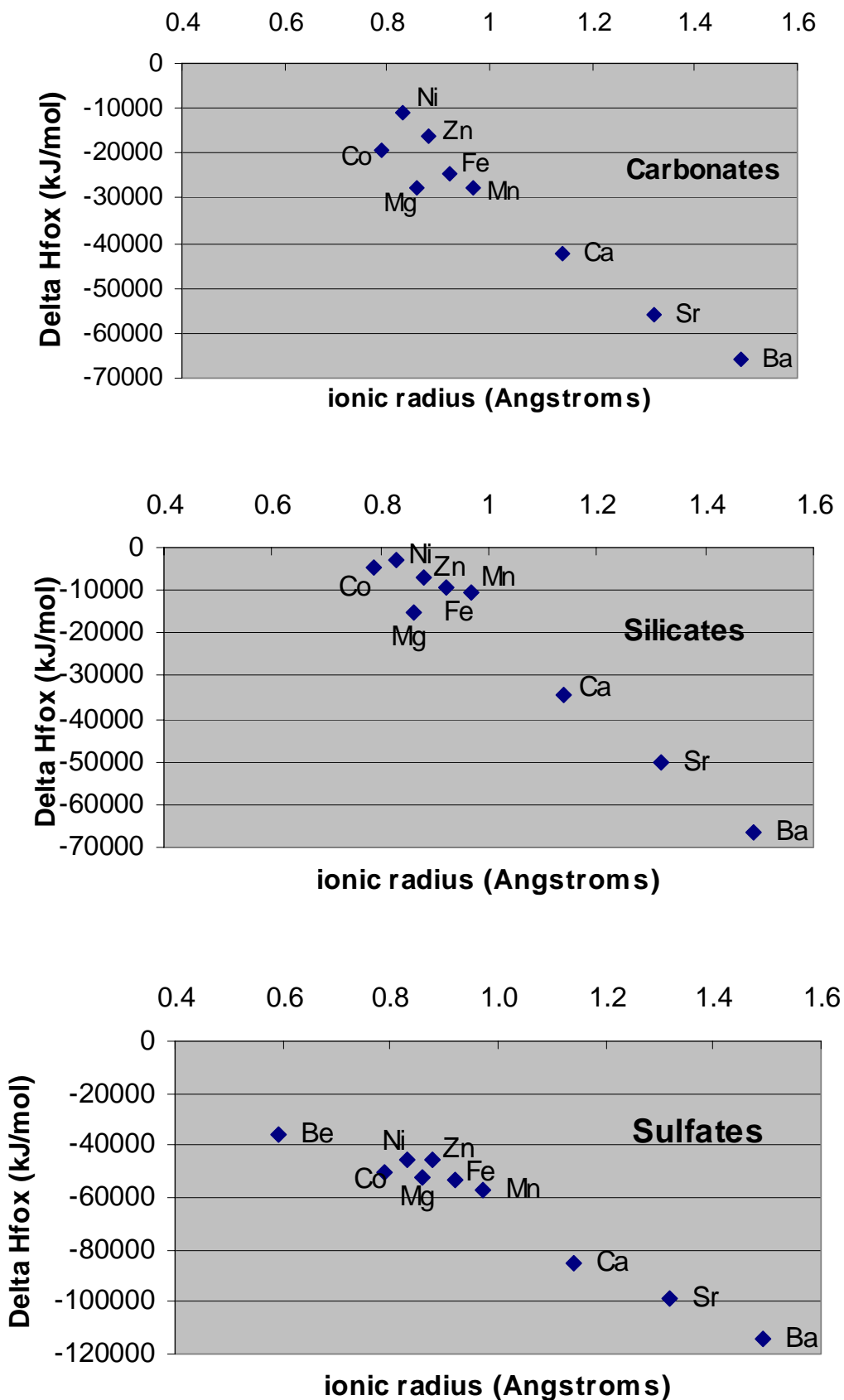


Figure 6. Correlation between heat of formation from the oxides and ionic radius for carbonate (MCO_3), orthosilicate (M_2SiO_4), and sulfate (MSO_4) compounds with divalent anions. Data taken from FACTSAGE thermodynamic database.